

# Segmentation of airborne hyperspectral images by integrating multi-level data fusion

M. Lennon, M.C. Mouchot, G. Mercier, B. Solaiman

Département ITI

ENST-Bretagne – BP 832

F-29285 Brest Cédex

Marc.Lennon@enst-bretagne.fr

L. Hubert-Moy

Laboratoire Costel

Université de Rennes 2- 6, avenue G. Berger

F-35043 Rennes Cédex

Laurence.Hubert@Uhb.fr

**Abstract** – *This paper deals with the extraction of the hedgerow and copse network from hyperspectral images acquired with the Compact Airborne Spectrographic Imager (CASI). The strategy of segmentation integrates several levels of data fusion allowing a decision to be taken concerning the membership of each pixel to the hedgerow and copse network from the large set of original data. The first level leads to quantifying the membership of each pixel to specific features of the network. It includes data fusion based on physical properties, geometric context-dependent fuzzy fusion with an original consistency measure and the geometric fusion of decisions. The second level is a fuzzy fusion of methods allowing the membership of each pixel to the network to be quantified. Finally, the third level involves post-processing the data with a context-dependent fusion of decisions to obtain the final map of the hedgerow and copse network.*

**Keywords:** Fuzzy fusion, context-dependent fusion, consistency measure, geometric fusion, hyperspectral, CASI, segmentation, bocage network.

## 1 Introduction

Since the launch of the first airborne hyperspectral imaging sensors in the 80's, this mode of imaging increased rapidly and a great number of sensors [1] and information extraction techniques appeared [2]. This type of imaging spectrometer allows a huge number of spectral bands to be collected for each element of the scene (up to several hundred), while spatial resolution can reach a few dm at ground. Spectral bands acquired by such sensors range from the blue ( $\approx 400$  nm) to the near infrared ( $\approx 900$  nm), some of them to the thermal infrared ( $\approx 2500$  nm). Advantages of such sensors are obvious: they allow very fine spatial and spectral features of natural elements to be obtained, and thus enable ecosystems to be studied with a great accuracy. The main drawback is the large amount of information to process in order to take a decision for a particular study. Many techniques developed by researchers in the hyperspectral domain, even though these techniques are not presented as such,

are nothing but data fusion at different levels, leading to computing a thematic feature for each pixel or region of the scene from the large set of original data. This paper shows these different levels of fusion including data fusion, parameter fusion methods and decision fusion in a thematic application with images from the CASI [3]. This pushbroom sensor allows images to be obtained in a spectral domain comprised between 400 and 900 nm with a spectral resolution of 2 nm. The spatial resolution can reach 0.5 m at ground. It can be operated in two modes: the spatial mode allowing 512 pixels to be obtained across the flight line with up to 40 spectral bands; the spectral mode allowing more spectral bands with less than 512 pixels to be obtained across the flight line (limit: 288 spectral bands, 16 pixel swath). CASI is here used for the study of diffuse pollution from agricultural activity. More specifically, the hedgerow and copse network is the landscape element under consideration. Its characterization presents a great interest in the study of this type of pollution because it is able to stop and absorb an important proportion of the water flux charged with pollution particules (nitrates, salts, etc) depending on its location, morphology, composition, direction, etc [4]. Conventional remote sensing techniques are limited for such a study: the spatial resolution of satellital sensors is too low and spectral information from aerial photography is too poor for an accurate characterization. The hedgerow and copse network needs first to be segmented from CASI images, the study under consideration in this paper. First, the acquisition process and data obtained will be presented; the strategy of segmentation based on fuzzy fusion will be explained. The use of the concepts of fuzzy fusion will be justified. Then, the preprocessing techniques will be presented. The computing of several attributes including fusion based on physical properties, geometric and context-dependent fusion techniques will be developed next. The last part concerns the fusion of methods and decision fusion for post-processing. Finally, the results and their exploitation are shown and discussed before the conclusion.

## 2 Image acquisition

Images were acquired in July 1998 above Plounérin, a bocage landscape located in the north of Brittany (France), largely diseased by agricultural pollution. The spatial resolution is 2 m at ground and pixels include 9 spectral bands ranging from 400 to 900 nm. The 5 flight lines acquired were corrected for the plane attitude (pitch, roll and yaw) and mosaïcked. A large region was then extracted to produce a single rectangular image of the scene. The size of the scene is approximately 1.1 km wide and 2.1 kms long. A color composition of this image is shown in *fig. 1* (Red : 799.9 nm, green : 677.7 nm, blue : 551.1nm). The network composed of hedges, banks and copses is visible.



Fig. 1 : CASI image color composition of Plounérin

## 3 Segmentation strategy

A segmentation strategy based only on the spectral features of the hedgerow and copse network would meet two main problems : on the one hand, spectral features are multiples depending on the composition of the hedges and on the other hand, they can be the same as other landscape elements such as fields for example. Hence, other discriminant features need to be determined. The first of

these is the texture. Although the spectral features of a group of bocage pixels is almost the same as a group of field pixels, their texture usually enables them to be discriminated. Moreover, the network is most often composed of linear structures. A shape attribute also needs to be extracted from the images. These concepts of radiometry, texture and shape are quite different but need to be merged in order to produce a satisfying segmentation. Because of the fuzzy nature of the problem and in order to homogenize these three different concepts, fuzzy fusion methods are used. Membership to each one of the three attributes is computed in parallel. Initially, the original radiance images should be calibrated to reflectance in order to allow the method to be reproducible. Because of the large variability in the spectral features of the original data, a filtering step is operated before the computing of the shape features. This step leads to a much less noisy result. On the other hand, the computing of the texture features must be operated on the original data set in order to take advantage of this variability. The result of this parallel step is a membership image to each of the 3 attributes. Fuzzy fusion concepts are used to merge them in a single image. In order to remove the noise from this image and to take a final decision, morphological post-processing using context-dependent decision fusion techniques is implemented. The complete scheme of segmentation is shown in *fig. 2*.

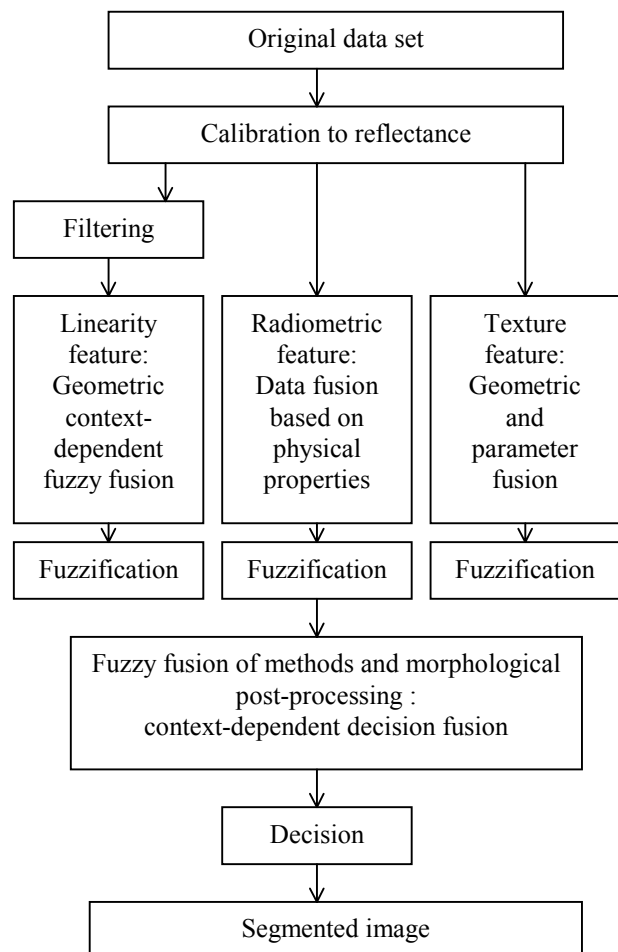


Fig. 2 : Global scheme of segmentation strategy

## 4 Preprocessing techniques

### 4.1 Calibration to reflectance

Because neither field spectrometry data nor atmospheric condition information is in our possession at the time of the acquisition of images, a simple calibration technique based on the information contained in the image is performed. It involves first scaling the radiance values in each image spectrum so that their sum is constant over the entire scene. This step largely removes shading effects and overall variations in brightness. Secondly, a uniform area having a relatively flat spectral reflectance curve is extracted from the image (roofs of agricultural buildings). The mean spectrum of such an area is dominated by the combined effects of solar irradiance and atmospheric scattering and absorption. The image is converted to relative reflectance by dividing each image spectrum by the flat field mean spectrum [5] [6].

### 4.2 Non linear filtering by hyperspectral anisotropic diffusion

The main idea of the isotropic diffusion involves observing that filtering an image with a Gaussian operator whose variance is  $\sigma^2$ , is equivalent to an image intensity local diffusion process during a time  $t$  which is proportional to  $\sigma^2$ . This principle comes from the heat diffusion phenomenon which balances the differences in concentration without changing the total mass [7]. Unfortunately, the isotropic diffusion smooths also the edges of the image. The anisotropic diffusion consists thus in highly diffusing in low gradient regions and lowly diffusing in high gradient regions. The image will thus be largely smoothed in relatively homogeneous regions while filtering will be stopped near the edges. A complete mathematical study of the theory can be found in [8]. The filtering is computed with the partial derivative equation (1):

$$\frac{\partial u}{\partial t}(x, y, t) = \text{div}(c(|\nabla u(x, y, t)|) \nabla u(x, y, t)) \quad (1)$$

Several functions  $c(|\nabla u|)$  have been proposed. We have chosen the function  $c(|\nabla u|)$  proposed by Weickert [9] for its convergence speed (2):

$$c(|\nabla u|) = 1 - \exp\left(-\frac{c_m}{(|\nabla u(x, y)|/k)^m}\right) \quad (2)$$

Weickert proposed taking  $m = 4$  and  $c_4 = 3.31$ .  $k$  is the threshold parameter and must be empirically fixed. Each image corresponding to each wavelength will be smoothed separately but we propose to take advantage of the multispectral information by computing the vectorial gradient (3):

$$|\nabla u(x, y)| = \left\| \nabla_{u_x}(x, y), \nabla_{u_y}(x, y) \right\|_2 \quad (3)$$

$$\text{With } \nabla_{u_x}(x, y) = \left\| \vec{u}(x, y), \vec{u}(x+1, y) \right\|_2$$

$$\text{and } \nabla_{u_y}(x, y) = \left\| \vec{u}(x, y), \vec{u}(x, y+1) \right\|_2$$

## 5 Radiometric feature : fusion based on physical properties

The hedgerow and copse network is always vegetal even if the amount of vegetation is not constant over the entire network. A simple vegetation coefficient is hence adequate to quantify the amount of vegetation for each pixel in the scene. This attribute is not sufficient because some fields are also vegetal but it will remove non-vegetal elements such as bare soil and man-made structures. The Transformed Vegetation Index (*TVI*) is computed (4). It is able to quantify the « red edge » representing the quantity of chlorophyll of the pixel under consideration, a physical property related to the amount of vegetation.

$$TVI = 100 \sqrt{\frac{u_{NIR} - u_R}{u_{NIR} + u_R}} \quad 0 < TVI < 100 \quad (4)$$

$u_{NIR}$  represents a band of image  $u$  in the near infrared while  $u_R$  represents a band of image  $u$  in the red wavelength. *TVI* can be seen as the fusion of spectral bands leading to a simple radiometric feature. In order to homogenize the three concepts, *TVI* is fuzzified by an S-Shape function (see *fig. 3*) to obtain the Radiometric Feature Membership (*RFM*).

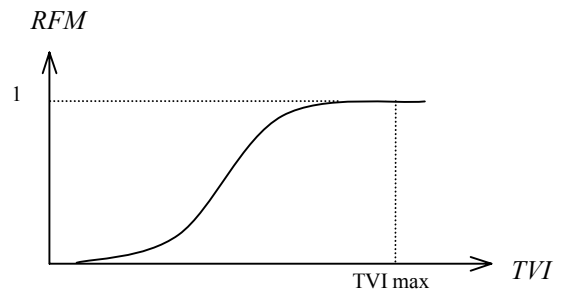


Fig. 3 – Membership function for RFM

## 6 Linearity feature : geometric context-dependant fuzzy fusion with original consistency measure

The following hypotheses are stated for a pattern to be a linearity feature:

H1 – A linearity feature can only be defined in its local context. The latter should neither be too large (the pattern cannot be approximated by a straight line, or many landscape patterns are present) nor too small (insufficient knowledge of the landscape configuration). Given the classical width of hedges, the size of the analysing window is fixed at 9 pixels (corresponding to 18 m at ground).

H2 – Linearity can be defined by one invariable state in one direction and at least three distinct invariable states in the three other directions (the present study is limited to four directions  $\theta_i$ ,  $i \in [N-S, E-W, NE-SW, NW-SE]$ ).

The number of states in one direction,  $NS(\theta_i)$ , will be quantified by the study of the evolution of the vectorial gradient of consecutive pixels  $|\sigma u(t)|$  in direction  $\theta_i$  ( $t \in [1,8]$  represents successive pairs of consecutive pixels in direction  $\theta_i$ ). Fig. 4 summarizes the evolution of  $|\sigma u(t)|$  for a perfect linearity.

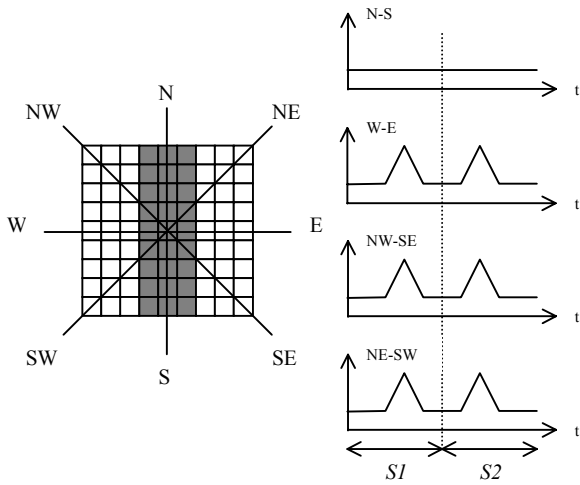


Fig. 4 – evolution of  $|\sigma u(t)|$  for a perfect linearity

If a pixel has at least one large gradient value on each of the two sides  $S_1$  and  $S_2$  of one direction  $\theta_i$ , then it will own three states in direction  $\theta_i$ . If a pixel has only small gradients on the two sides of one direction  $\theta_i$  then it will own only one state in direction  $\theta_i$  (5).

$$NS(\theta) = \text{Min} \left( \text{Max}_{t \in S_1} (|\nabla u(t)|), \text{Max}_{t \in S_2} (|\nabla u(t)|) \right) \quad (5)$$

Membership to three states in direction  $\theta_i$ ,  $\mu_3(\theta_i)$ , will be computed by a linear membership function bounded by the maximum value of  $NS(\theta_i)$  in direction  $\theta_i$  (fig. 5). Membership to one state  $\mu_1(\theta_i)$  is the inverse of membership to three states  $\mu_3(\theta_i)$ .

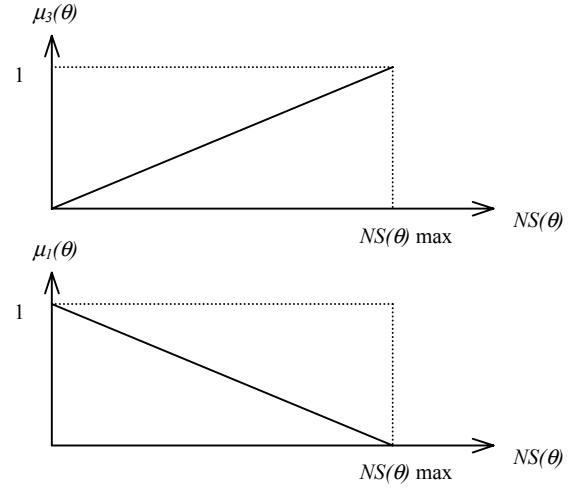


Fig. 5 – Membership functions for  $\mu_1(\theta_i)$  and  $\mu_3(\theta_i)$

Given H2, The *min* operator could be used to compute the degree of linearity in each of the four directions  $i$  (6).

$$\mu_L(\theta_i) = \text{Min}(\mu_1(\theta_i), \mu_3(\theta_j), \mu_3(\theta_k), \mu_3(\theta_l)) \quad (6)$$

Unfortunately, the *min* operator leads to a too restrictive result whereas the *max* operator is too lenient. We thus propose using a context-dependent operator [10] allowing variation between *min* and *max* depending on a consistency measure  $\sigma$  [11],  $\sigma \in [0,1]$ . Computation of the degree of linearity with  $\sigma$  is given in (7) :

$$\mu_L(\theta_i) = \sigma \text{Min}(\mu_1(\theta_i), \mu_3(\theta_j), \mu_3(\theta_k), \mu_3(\theta_l)) + (1 - \sigma) \text{Max}(\mu_1(\theta_i), \mu_3(\theta_j), \mu_3(\theta_k), \mu_3(\theta_l)) \quad (7)$$

We define  $\sigma$  as in (8) :

$$\sigma = f(\alpha(\mu_1(\theta_i), \mu_3(\theta_j), \mu_3(\theta_k), \mu_3(\theta_l))) \quad (8)$$

With  $\alpha \in [0, 45^\circ]$  being the spectral angle in the 4-dimensional space between vectors  $V_\mu = [\mu_1(\theta_i), \mu_3(\theta_j), \mu_3(\theta_k), \mu_3(\theta_l)]$  and  $V_C = [C, C, C, C]$  with  $C = cte$ .  $V_C$  represents the maximal consistency between the four parameters ( $\mu_1(\theta_i) = \mu_3(\theta_j) = \mu_3(\theta_k) = \mu_3(\theta_l)$ ). Let us define  $f$  as a monotone linear decreasing function (fig. 6.a).

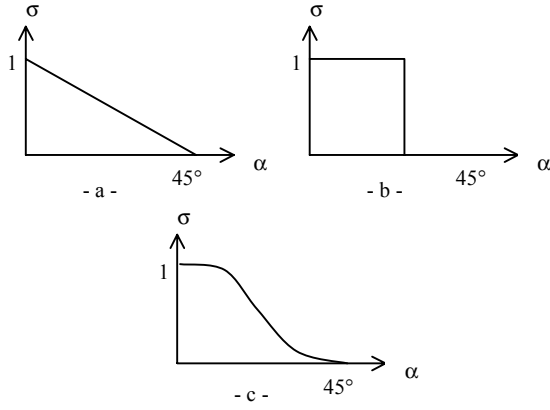


Fig. 6 – Different functions  $\sigma = f(\alpha)$

Note that, depending on applications,  $f$  could be chosen as a threshold function (fig. 6.b), or as a shape function (fig. 6.c) whose parameters of each function (threshold and curve, respectively) could be controlled, leading to the possibility of adapting the consistency depending on a second context parameter (i.e. in a noisy context, restriction should perhaps be higher even if consistency is high). Finally, from H2, a pixel is considered linear if it is linear in at least one direction (9). This leads to the final computation of the Linear Feature Membership (LFM).

$$LFM = \text{Max}_i(\mu_L(\theta_i)) \quad (9)$$

## 7 Texture feature: geometric and parameter fusion

We propose extending the cooccurrence method [12] to the n-dimensional case of hyperspectral images. 14 parameters were derived from the cooccurrence matrix in two dimensions. We propose an n-D extension to the two most interesting ones for our study : Correlation ( $Cr$ ) and Local Homogeneity ( $Lh$ ). A 3-pixel square window is chosen for the analysis. The module of cooccurrence vector is 1 pixel and its directions are the same four as in the study of linearity (fig. 4).  $Lh$  is computed as in (10) :

$$Lh(\theta_i) = \sum_{\vec{v}_1} \sum_{\vec{v}_2} \frac{1}{1 + \alpha^2(\vec{v}_1, \vec{v}_2)} \cdot CM_t(\vec{v}_1, \vec{v}_2) \quad (10)$$

$\vec{v}_1, \vec{v}_2$  : 2 vectors separated by cooccurrence vector  $t(\theta_i)$

$\alpha(\vec{v}_1, \vec{v}_2)$  : spectral angle between  $\vec{v}_1$  and  $\vec{v}_2$

$CM_t(\vec{v}_1, \vec{v}_2)$  : number of cooccurrences between  $\vec{v}_1$  and  $\vec{v}_2$

Note : given the huge dynamic of hyperspectral images,  $CM_t$  will almost always be equal to 1. The fusion rule adopted is the following one : a pixel is in a local homogeneous region if local homogeneity is high in every direction (11).

$$Lh = \text{Min}_i(Lh(\theta_i)) \quad (11)$$

Weighted means  $m$  and standard deviations  $\sigma$  of lines  $x$  and columns  $y$  of  $CM_t$  are needed for computing  $Cr(\theta)$ . With the assumption that  $CM_t$  is almost always equal to 1, we make the approximation that  $m = m_x = m_y$  and  $\sigma = \sigma_x = \sigma_y$ . Computing  $m$  and  $\sigma$  in the local context of size  $3 \times 3$  does not lead to obtaining discriminant correlation coefficients. Correlation is not representative of the local context if  $m$  and  $\sigma$  are computed over the entire image. Hence,  $m$  and  $\sigma$  are computed in a window  $W$  of intermediate size. A size of 81, chosen empirically is a good compromise. However, to compute statistics in a window of size 81 around every pixel is too expensive in computing time. We thus choose to pre-compute statistics in windows  $W_k$  with a recovery rate of 80%. This leads to an acceptable computing time and error rate. The procedure of computing is finally the following (12) :

$$\begin{aligned} \vec{v}_{moy}(k) &= \frac{1}{81^2} \sum_i \sum_j \vec{v}(i, j) \\ \vec{v}_\sigma(k) &= \sqrt{\frac{1}{81^2} \sum_i \sum_j (\vec{v}(i, j) - \vec{v}_{moy}(k))^2} \quad i, j \in W_k \\ Cr(\theta_i, W_k) &= \frac{1}{|\vec{v}_\sigma(k)|^2} \sum_{\vec{v}_1} \sum_{\vec{v}_2} \left\| \vec{v}_1, \vec{v}_{moy}(k) \right\|_2 \times \\ &\quad \left\| \vec{v}_2, \vec{v}_{moy}(k) \right\|_2 \times CM_t(\vec{v}_1, \vec{v}_2) \quad (12) \end{aligned}$$

with :

$\vec{v}_1, \vec{v}_2$  : 2 vectors separated by cooccurrence vector  $t(\theta_i)$

$CM_t(\vec{v}_1, \vec{v}_2)$  : number of cooccurrences between  $\vec{v}_1$  and  $\vec{v}_2$

Fusion rule : a region is said to be correlated if the correlation is high in every window  $W_k$  and in every direction  $\theta_i$  (13).

$$Cr = \text{Min}_i \left( \text{Min}_k (Cr(\theta_i, W_k)) \right) \quad (13)$$

Correlation and local homogeneity are fuzzified with S-Shape functions (fig. 7).

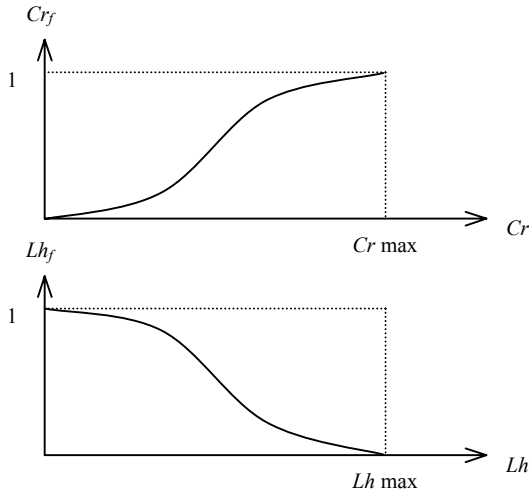


Fig.7 – Membership functions for  $Cr$  and  $Lh$

In order to perform the fusion of both parameters, we state the hypothesis that a pixel has a good texture feature if correlation is high and local homogeneity is low. The Texture Feature Membership ( $TFM$ ) is hence assumed to be equal to the disjunction of the two membership images (14) :

$$TFM = Min(Cr, Lh) \quad (14)$$

Finally, morphological grey-level closure is performed to smooth noise from  $TFM$ .

## 8 Method fusion and morphological post-processing with context-dependent decision fusion

The three different methods provided the memberships to features of radiometry ( $RFM$ ), linearity ( $LFM$ ) and texture ( $TFM$ ). We state the hypothesis that a pixel belongs to the hedgerow and copse network if it is radiometrically correct and linear (hedges and banks) or if it is radiometrically correct and its texture feature membership is high (copses). Hence, the first step of the fusion method allows results from the three methods ( $RFM$ ,  $LFM$ ,  $TFM$ ) to be merged to two new fuzzy variables :  $RLFM$  (Radiometry-Linearity Feature Membership) and  $RTFM$  (Radiometry-Texture Feature Membership) with the simple  $min$  operator (15) :

$$\begin{aligned} RLFM &= min(RFM, LFM) \\ RTFM &= min(RFM, TFM) \end{aligned} \quad (15)$$

However, these two new membership images are noisy and post-processing is necessary in order to free the final decision from holes or isolated pixels. The context needs first to be defined. Depending on this context, different morphological post-processing will be performed. The radiometry feature membership of the pixel under consideration should be high. This assumption provides the first rule allowing the context to be defined. The first decision concerning the context thus involves thresholding

the  $RFM$ . If this step gives the decision that the radiometry feature is bad, then no action will be performed. If it gives the decision that the radiometry feature is good, then the context needs to be more accurately defined. This leads to the second rule allowing the context to be defined. The latter should determine whether the grey level mean of a region is high or low. A low and a high threshold,  $Tl$  and  $Th$ , are then fixed empirically. A circular region around the pixel is defined. In the first step, the radius of the disc is fixed at one pixel. If the mean grey level of the circular region around the pixel is comprised between the low and high threshold, then the radius of the disc is incremented and the mean grey level of the new region is computed. The process is performed iteratively until the mean grey level of the region becomes lower than the low threshold or higher than the high threshold or until the size of the region becomes too large (the maximum size of the context is fixed at a sphere radius of 10 pixels). Fig. 8 illustrates this process.

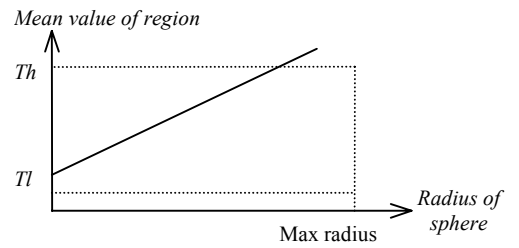


Fig. 8 – Evolution of the context feature with respect to its size

At the end of the process, the distance between the mean value of the region and the high threshold ( $d1$ ) and the distance between the mean value of the region and the low threshold ( $d2$ ) are compared. If  $d1 < d2$ , the decision is taken that the grey level mean of the region is high. If  $d2 < d1$ , the decision is taken that the grey level mean of the region is low. This process gives another result: the size of the region needed to determine the context. In order to remove too small and isolated detected structures, grey level morphological erosion will be performed if the grey level mean of the region is low. In order to remove holes in the detected structures, grey level morphological dilatation will be performed if the grey level mean of the region is high. Both morphological operations are computed with a structuring element given by the size of the region which was needed to determine the context. To resume, from the fusion of the two rules allowing the context to be defined (radiometry and mean grey level) and the two decisions (erosion and dilatation), the final post-processed  $RLFM$  (called  $RLFM_{pp}$ ) and  $RTFM$  (called  $RTFM_{pp}$ ) are computed. A simple  $max$  operator allows these fuzzy variables to be merged to obtain the hedgerow and copse network membership image  $S$  (16) :

$$S = Max(RLFM_{pp}, RTFM_{pp}) \quad (16)$$

The final decision is computed thanks to a simple threshold of  $S$  and a hole filling on the binary image to remove the last noisy structures. This leads to the final segmented image illustrated in *fig. 9*. One can notice that fields and man-made structures have been removed (white pixels) and only the hedge and copse network is present (black pixels).



Fig. 9 – Final bocage network segmented image (black pixels)

## 9 Discussion about methods and results – further work

Let us discuss the results for each step of the segmentation strategy: after calibration to reflectance, the first step is the anisotropic diffusion filtering allowing the effects of noise to be decreased while processing the detection of linear structures. We proposed taking advantage of the multispectral information by computing the vectorial gradient, a method leading to promising results. However, results could probably be improved by using a « more intelligent » adaptive function taking into account specific features of the transitions between the hedgerow and copse network and other landscape patterns. Our research is currently into this direction. A more sophisticated study of radiometric features could be performed even if the goal, here, is not to produce an accurate classification, but merely to quantify the sufficient quantity of vegetation

required for a pixel to be a candidate to the hedgerow and copse network election. Concerning the study of the linearity feature, fusion rule (5) leading to the computation of  $NS(\theta)$  from the evolution of the vectorial gradient  $|\sigma_u(t)|$  could be improved in order to be more robust to the noise. A local context adaptive fusion rule could be implemented. The original method which was proposed to compute the consistency measure  $\sigma$  (8) with an  $n$ -D spectral angle  $\alpha$  and associated function  $f$  leads to promising results. It can be applied in many domains where the fusion of  $n$  fuzzy variables must be adapted to the local context. The method even allows a hierarchy of several functions characterizing different features of the context to be built. The following gives an example :  
 Let  $F1$  be the first feature of the context (i.e. color)  
 Let  $F2$  be the second feature of the context (i.e. noise)  
 Let  $\alpha$  be the consistency between the  $n$  fuzzy variables computed with the spectral angle method.  
 The context-dependent operator  $\sigma$  can be computed as in (17) :

$$\sigma = f1(f2(\alpha)) \quad (17)$$

The parameters of functions  $f1$  and  $f2$  can be controlled by features  $F1$  and  $F2$ .

In the analysis of the texture feature, more parameters from cooccurrence matrices could be extended to  $n$  dimensions leading to the possibility of discriminating more complex hyperspectral textures. Rather than computing parameters in fixed-size windows, region growing methods could be performed. In such methods, new fusion rules would have to be determined. This approach forms part of our current research. Concerning the post-processing of data, the rules allowing the features of the context to be quantified could be improved. The use of a growing surface whose borders would adapt to the context would perhaps lead to better results than the growing disc used even if current results are promising. Even if the methods can be improved in the several levels of fusion, global results are promising and enable the production of a segmented image largely exploitable for further characterization.

## 10 Results exploitation

The second part of the work, not presented in this paper, involves quantitatively characterizing the hedgerow and copse network. A morphological study of the segmented image enables width and direction of hedges to be computed for each pixel of the network. With the help of a digital elevation model of the same region, five parameters are computed: module and direction of the slope, distance to the river by the direct route and by the drainage route, and water flux accumulation. An accurate study of the spectral features of the original image in the segmented region enables a classification of vegetal species which exist in the hedgerow and copse network. This set of parameters is valuable for environment managers who have to find methods to control the pollution.

## 11 Conclusions

The extraction of relevant information from large set of data included in hyperspectral images is not a trivial task. This work showed how some concepts of fuzzy data fusion can be used at different levels (data, parameters, methods, decisions) to segment specific landscape patterns. Conventional techniques such as min-max have been used in conjunction with original context-dependent methods. The latter present an interest for many applications as far as data fusion is concerned.

## References

- [1] Michael Schaepman, *List and characteristics of airborne imaging spectrometers*, [http://www.geo.unizh.ch/~schaep/research/apex/is\\_list](http://www.geo.unizh.ch/~schaep/research/apex/is_list).
- [2] D. Landgrebe, *Information extraction principles and methods for multispectral and hyperspectral image data*, Information processing for remote sensing, C.H. Chen Ed., World Scientific Publishing Co., USA, 1999.
- [3] *Information on CASI sensor*, <http://www.itres.com>.
- [4] L. Hubert-Moy, A. Cottonnec, P. Gouery, *Extraction du réseau bocager à l'aide de données satellitaires Landsat Thematic Mapper. Application à un bassin versant en Bretagne centrale*, Photo-Interprétation, 4 :258--263,1995.
- [5] R.B. Smith, *Getting started : analysing hyperspectral images with TNTmips*, 30--32, <http://www.microimages.com>.
- [6] F.H. Goetz, J.W. Boardman, *Atmospheric corrections : on deriving surface reflectance from hyperspectral imagers*, Imaging Spectrometry III, Proceedings of SPIE, 3118, 14--22.
- [7] R. Deriche, O. Faugeras, *PDE's in image processing and computer vision*, Traitement du Signal, 13(6), 1996.
- [8] B.M. ter Haar Romeny, *Geometry-driven diffusion in computer vision*, Kluwer Academic, Dordrecht, 1994.
- [9] J. Weickert, *Anisotropic diffusion in image processing*, PhD thesis, University of Kaiserslautern, Germany, Laboratory of Technomathematics, January 1996.
- [10] I. Bloch, *Information combination operators for data fusion : a comparative review with classification*, IEEE Transactions on Systems, Man and Cybernetics, 26(1), 52-67, 1996.
- [11] R. Yager, A. Kelman, *Fusion of fuzzy information with considerations for compatibility, partial aggregation and reinforcement*, International journal of approximate reasoning, 15, 93--122, 1996.
- [12] R.M. Haralick, *Statistical and structural approaches to texture*, Proceedings of the IEEE, 67(5), 786--804, 1979.